Subangstrom Edge Relaxations Probed by Electron Microscopy in Hexagonal Boron Nitride

Nasim Alem,[1,2,3] Quentin M. Ramasse,[4,*,†] Che R. Seabourne,[5] Oleg V. Yazyev,[1,3,6] Kris Erickson,[1,3]
Michael C. Sarahan,[4] Christian Kisielowski,[7] Andrew J. Scott,[5] Steven G. Louie,[1,3] and A. Zettl[1,2,3,*,‡]

[1]*Department of Physics, University of California Berkeley, Berkeley, California 94720, USA*

[2]*Center of Integrated Nanomechanical Systems, University of California Berkeley, Berkeley, California 94720, USA*

[3]*Materials Sciences Division, Lawrence Berkeley National Laboratory, Berkeley, California 94720, USA*

[4]*SuperSTEM Laboratory, STFC Daresbury, Keckwick Lane, Daresbury WA4 4AD, United Kingdom*

[5]*Institute for Materials Research, SPEME, University of Leeds, Leeds LS2 9JT, United Kingdom*

[6]*Institute of Theoretical Physics, Ecole Polytechnique Fédérale de Lausanne (EPFL), CH-1015 Lausanne, Switzerland*

[7]*National Center for Electron Microscopy and Joint Center for Artificial Photosynthesis,
Lawrence Berkeley National Laboratory, Berkeley, California 94720, USA*

Theoretical research on the two-dimensional crystal structure of hexagonal boron nitride (*h*-BN) has suggested that the physical properties of *h*-BN can be tailored for a wealth of applications by controlling the atomic structure of the membrane edges. Unexplored for *h*-BN, however, is the possibility that small additional edge-atom distortions could have electronic structure implications critically important to nanoengineering efforts. Here we demonstrate, using a combination of analytical scanning transmission electron microscopy and density functional theory, that covalent interlayer bonds form spontaneously at the edges of a *h*-BN bilayer, resulting in subangstrom distortions of the edge atomic structure. Orbital maps calculated in 3D around the closed edge reveal that the out-of-plane bonds retain a strong π^* character. We show that this closed edge reconstruction, strikingly different from the equivalent case for graphene, helps the material recover its bulklike insulating behavior and thus largely negates the predicted metallic character of open edges.

The atomic structure of two-dimensional crystal membranes can modulate their electronic, magnetic, and optical properties, making these materials desirable for a variety of applications [1,2]. For example, zigzag graphene nanoribbons were recently predicted to realize controllable half-metallic electronic structure, with tantalizing potential for spin-based electronic devices on the nanometer scale [3]. Atomically thin sheets of hexagonal boron nitride (*h*-BN) possess an atomic structure analogous to graphene, but with drastically different electronic properties. The atomic arrangement of *h*-BN consists of alternating boron and nitrogen atoms forming a honeycomb structure. The individual sheets of *h*-BN are stacked with the boron atoms residing on top of the nitrogen atoms, with no offset within a column. Although structurally pristine sheets of *h*-BN maintain a band gap larger than 5 eV, edges and defects in an *h*-BN membrane can dramatically modify the electronic structure of this two-dimensional material by introducing in-gap states [4,5]. *h*-BN nanoribbons with certain edge geometries and termination have even been theorized to have local magnetic moment [6]. Therefore, similar to graphene, modulations in the atomic structure of *h*-BN can help tailor its properties for a variety of applications, especially within the field of spintronics.

Recent advancements in ultrahigh resolution aberration-corrected electron microscopy have opened up the possibility of studying the local structure and bonding of two-dimensional materials one atom at a time [7–10]. Beyond the mere technical prowess, we show here that these techniques can be applied to concrete and complex issues in materials design: we have used state-of-the-art scanning transmission electron microscopy (STEM) and electron energy loss spectroscopy (EELS) to observe and analyze subangstrom structural relaxations that take place at the edges of an *h*-BN bilayer. Coupling such precise experimental data with first-principles calculations has lead us to the discovery of new physical effects in *h*-BN. This study shows that the edge atoms undergo an unusual distortion that is strikingly different from bilayer graphene. Calculated 3D orbital maps as well as the unoccupied density of states probed by EELS have not only uncovered the nature of bonding at the distorted *h*-BN edges, but also rationalized the changes in the core-level EELS spectra in a novel fashion. We show that covalent interlayer B-N bonds are spontaneously formed across the adjacent layers, resulting in a structure analogous to a folded single-layer *h*-BN. This reconstruction thus restores the electronic properties expected for a single-layer *h*-BN with no edge effects. Understanding such underlying physical and chemical effects is very important in nanoengineering two-dimensional crystals, such as *h*-BN and *h*-BN/graphene hybrids, for desirable physical and electronic properties.

Figure 1 shows an annular dark field (ADF) STEM image of the edge of a bilayer *h*-BN sheet obtained by
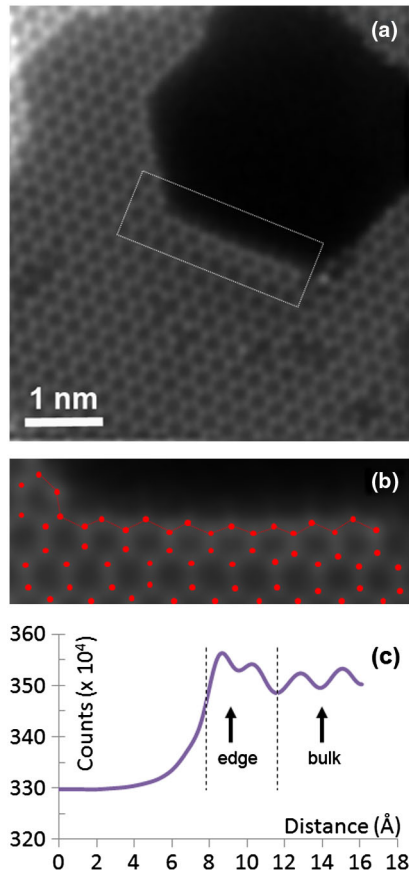
FIG. 1 (color online). Imaging structural relaxations at the edge of bilayer *h*-BN. (a) Annular dark field STEM image of a large bilayer *h*-BN sheet showing a hole with straight zigzag edges. (b) The individual atoms at the magnified *h*-BN edge are marked with red dots. A distortion pulls the zigzag edge atoms away from the hole creating a curvature at the edge. (c) The intensity at the edge of the bilayer is increased, while no impurities or adatoms were found to reside at this part of the edge.

mechanical exfoliation from *h*-BN powder (see Supplemental Material [11]). This area shows the formation of zigzag edges and a bilayer of *h*-BN next to the hole. During the growth of the hole in this region, narrow monolayer step edges were observed next to the hole before the monolayer atoms were further sputtered away. Such intensity variation around the hole confirmed the presence of bilayer *h*-BN in this region of the sample. The micrograph was processed using a maximum entropy-based probe deconvolution algorithm to improve noise levels (see Supplemental Material [11] for details on the image processing). Even though this work was carried out under so-called ''gentle STEM conditions'' (high vacuum at the sample below 5×10^{-9} Torr, 60 keV primary beam energy) [12], *h*-BN remains beam sensitive and ultimately holes can be created in the middle of the membrane during imaging via knock-on damage from the electron beam. In addition to holes whose edges (predominantly of the ''zigzag'' type) are stable enough

for prolonged observation (at least over a few minutes), this process also results in the formation of boron monovacancies, which can be readily observed in Fig. 1 (see also the Supplemental Material [11] for further illustration). Remarkably, the higher magnification image of the region near the newly formed hole in the bilayer *h*-BN in Fig. 1(b) shows that the atoms located immediately at the edge of the membrane, marked with red dots, exhibit considerable in-plane contraction relative to the bulk *h*-BN lattice. In addition to the obvious structural distortions, the edge atoms also show an increase in contrast [Fig. 1(c)], although EELS does not show any evidence of impurities or adatoms residing at the bright edge in this region of the sample.

We have used density functional theory (DFT) calculations to elucidate the local edge structure at the bilayer *h*-BN (see Supplemental Material [11]). Figure 2(a) shows a schematic model in cross-sectional and plan views representing the predicted distortions at the edge of the bilayer *h*-BN. This figure shows a model of a bilayer *h*-BN nanoribbon with two edges: one is forced to maintain its pristine, ''bulklike'' structure [Fig. 2(a), bottom part] while the top edge of the membrane is allowed to minimize its energy through structural relaxation [Fig. 2(a), upper part] in a three-dimensional space. The calculated structural relaxations result in interlayer covalent bonds forming across the bilayer zigzag edge leading to a ''closed''
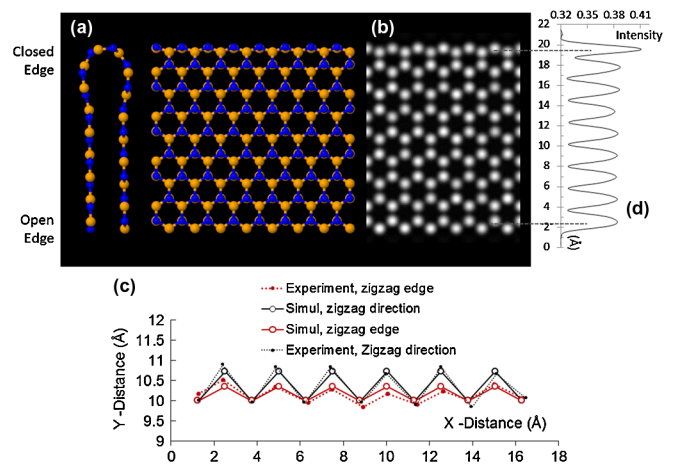

FIG. 2 (color online). Image simulations using the calculated structures for closed and open edges. (a) Cross-sectional and plan view schematics of a predicted DFT model showing the formation of interlayer bonds at the zigzag edges of a bilayer *h*-BN, resulting in local three-dimensional atomic displacements. (b) A simulated ADF-STEM image from the predicted DFT model. (c) Experimental and simulated in-plane atomic coordinates are compared with and without distortion in the zigzag direction. The relaxed edges in the experiment [Fig. 1(b)] precisely follow the predicted edge distortions from first-principles calculations of closed edges. (d) The relaxed (closed) edge of the simulated structure on the top shows enhanced intensity contrast compared to the pristine (open) edge.

edge termination. Our calculations predict an energy gain
of -4.9 eV for each interlayer bond formed at the edge.
Although these interlayer bonds in the out-of-plane direc-
tion have a covalent nature similar to the intralayer in-
plane sp^2 hybridized bonds within the bulk material, the
curvature at the edge leads to hybridization between σ and
π symmetry states.

The calculated structural model in Fig. 2(a) was used to
simulate an annular dark field STEM image using experi-
mental parameters (see the Supplemental Material [11]).
Figure 2(b) shows the simulated ADF-STEM image of
this model. On the top, the edge atoms undergo in-plane
distortion, while no structural distortion occurs on the
bottom edge. Figure 2(c) compares the in-plane distor-
tions observed between the experiment [Fig. 1(b)] and
simulations [Fig. 2(a)]. The black profiles show the atom
positions along the zigzag direction with no distortion,
while the red profiles represent the relaxed edge from
both experiment and simulation. The in-plane atomic
relaxations at the edge of the bilayer h-BN show excellent
agreement between the experiment and the simulation.
This relaxation arises from an in-plane atomic distortion
of 37 pm due to the formation of interlayer bonds along
the z direction. DFT calculations predict an out-of-plane
distortion of 96 pm for each edge-atom resulting in an
interlayer B-N bond length of 146 pm across the bilayer,
typical for the B-N bond length within the plane of sp^2
bonded h-BN. Local structural distortions of the same
nature and magnitude have been previously observed at
the h-BN membrane edges [13], BN helical cones [14],
as well as boron monovacancies in bilayer h-BN [7]
with nitrogen edge atoms shifting by 37 pm in the in-
plane direction and over 100 pm in the out-of-plane
direction from their pristine position. In the case of re-
laxed edges in bilayer h-BN, this atomic displacement
can significantly alter the channeling conditions for
STEM imaging, leading to a contrast increase, observed
experimentally and reproduced here in the image simula-
tions [Fig. 2(d)].

Additionally, the edge reconstruction and more specifi-
cally the formation of a direct interlayer B-N bond are
expected to result in important changes in the electronic
configuration of the h-BN membrane edge, relative to the
undistorted "bulk" or the undistorted "edge." These ef-
fects are probed by recording electron energy loss spectra
from individual atom columns. Figure 3 shows an annular
dark field image of the edge of the bilayer h-BN along with
boron K edges for the atom columns with identical chem-
istry on the edge and in the middle of the membrane. A
distinctly different fine structure for the boron K edge is
observed for the atom columns on the edge and within the
bulk in our experiment, most readily seen by a reversal of
the π^* to σ^* peak intensity ratio [Fig. 3(c)]. Figure 3(c)
compares experimental and simulated EELS spectra
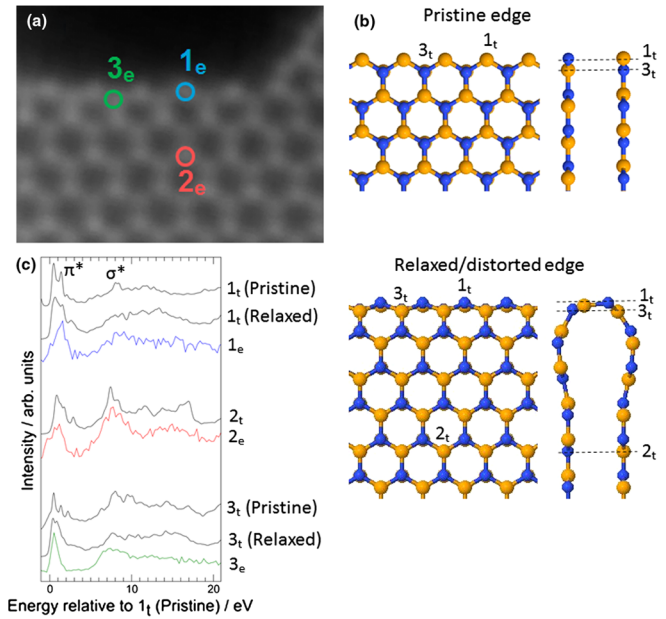(indicated by the subscripts "e" for experiment and "t"

FIG. 3 (color online). Experimental and simulated EELS data
along with annular dark field (ADF) images of bilayer h-BN at
the edge. (a) ADF image of bilayer h-BN at the edge along with
its EELS spectra at points 1_e, 2_e, and 3_e. Please note that a
different image was used to position the beam for spectrum 3_e.
The label 3_e indicates an "equivalent" atomic column, while the
actual beam location image is provided in the Supplemental
Material [11]. (b) Cross-sectional and plan view of the pristine
and relaxed models of bilayer h-BN edge. The dashed lines on
the cross-sectional schematics correspond to the atomic columns
1_t, 2_t, and 3_t for the pristine and relaxed edge models. (c) The
experimental and simulated EELS spectra at points 1, 2, and 3
already marked on images (a) and (b). Subscript e stands for
experiment and t for theory.

for theory) for two atomic column positions on the edge
[labeled "1" and "3" on the ADF image of Fig. 3(a)] and
one position away from the edge [labeled "2" on the ADF
image of Fig. 3(a)]. It should be noted that although the
image on Fig. 3(a) was recorded immediately prior to the
acquisition of EELS spectra 1_e and 2_e, another image was
used to position the beam for EELS spectrum 3_e. For visual
conciseness, the label on Fig. 3(a) indicates an equivalent
position at the edge of the sample; the actual location of the
beam for spectrum 3_e can be found in the Supplemental
Material [11].

Simulations were carried out on equivalent atom col-
umns using either the calculated "relaxed" (closed) edge
of a bilayer h-BN, or "pristine" (open) model in which
no interlayer bonding takes place. Positions 1_t, 2_t, and 3_t
on Fig. 3(c) were considered equivalent to the positions 1_e,
2_e, and 3_e in the simulations for both the pristine and
relaxed edge structures. As can be seen in Fig. 3(c), the
near-edge fine structure from positions 1_e and 2_e in
Fig. 3(a) matches remarkably well with the fine structure
predicted by the first-principles calculations carried out on

the atom columns 1_t (relaxed) and 2_t (relaxed) for the relaxed edge model. In addition, the experimental EELS spectra acquired on the atom columns 1_e and 3_e also show a similar fine structure to the simulated EELS spectra obtained from atom columns 1_t (relaxed) and 3_t (relaxed) in the relaxed edge model. By contrast, when comparing with the pristine structure, there is a significant difference between the fine structure of the experimental EELS spectra at points 1_e and 3_e and the simulated EELS spectra on the 1_t (pristine) and 3_t (pristine) atom columns. This comparison unambiguously validates the proposed relaxed (closed) edge model, and confirms the formation of interlayer bonds at the relaxed edge of the bilayer h-BN. Both experiments and simulations show a significantly higher π^* to σ^* ratio of the boron K edge (positions 1_e and 3_e) on the edge of the relaxed structure when compared to the bulk (position 2_e). In electronic structure terms this observation points to a higher contribution to the unoccupied density of states of the material of π^* orbital character at the edge of the sample, while away from the edge, the σ^* orbital contribution is more dominant.

Figure 4 presents an unoccupied orbital map for the π^* energy region as defined by the bulklike position 2 in Fig. 3. The map consists in a density plot of all unoccupied theoretical orbitals with energy entirely within the π^* region for atom 2; it is a three-dimensional data set and only a representative cross-sectional slice is shown, from the plane indicated on Fig. 4(a). The map shows that the π^* orbitals retain a significant density around the distortion even though they lie in an in-plane direction with respect to the membrane, a direction along which they are normally very weak in the bulk. Furthermore, the absolute orbital intensity is larger at the distortion as compared to the middle of the membrane. This could be directly related to the experimental observation that at the relaxed edge the π^* peak intensity is significantly increased relative to the σ^* peak. In addition, it might further suggest an enhanced preference for electrons to undergo transitions to π^* orbitals at the distortion as compared to the middle of the membrane. Such behavior is also observed around the curved walls of carbon nanotubes at large collection angles [15,16]. The geometry of the reconstructed edge of a bilayer h-BN sheet could be compared locally to a BN nanotube with an extremely short radius of curvature. We therefore suggest that the change of directionality with respect to the beam of the π^* orbitals along the interlayer bonds forming at the relaxed edges of h-BN gives rise to this shift in the transition of electrons into π^* as opposed to σ^* orbitals observed in the EELS.

This newly understood behavior may in turn have profound implications for tailoring the electronic properties of h-BN-based nanostructures. Figure 5 shows the computed band structure of bilayer h-BN nanoribbons with open and closed edges compared to the band structure of bulk bilayer h-BN calculated using the supercell dimension which corresponds to the nanoribbon models (see the Supplemental Material [11]). While bulk bilayer h-BN is characterized by a large band gap [4.4 eV within the present level of theory, see Fig. 5(a)], open edges introduce localized states in the gap, essentially making the edges metallic [Fig. 5(b)]. By closing the edges, bilayer h-BN saturates dangling bonds thus recovering the large band gap of bulk bilayer h-BN. Additionally, we find that the
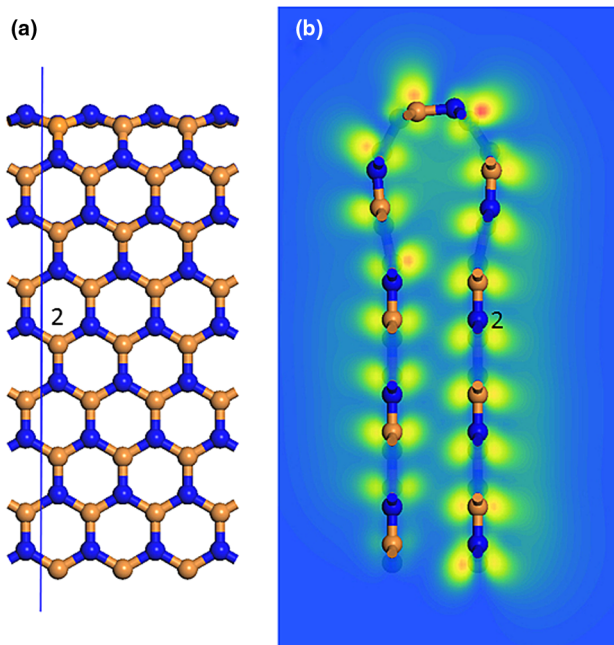

FIG. 4 (color online).   Orbital map of the closed bilayer edge. (a) Depiction of the cross-sectional slice at which unoccupied orbitals have been plotted (b) EELS unoccupied orbital map, illustrating the unoccupied orbitals which have energy windows lying within the π^* region for the bulklike position 2. Colors towards the red end of the spectrum indicate greater orbital intensity.
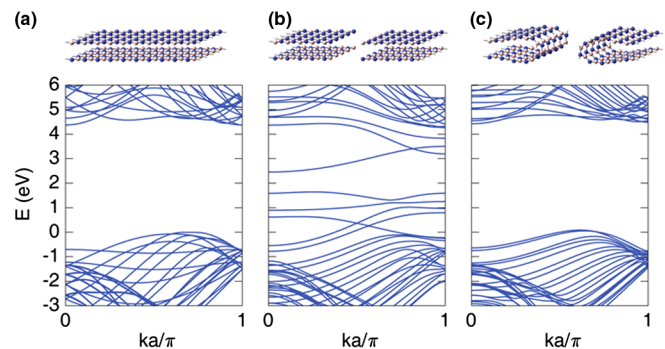

FIG. 5 (color online).   Calculated electronic band structures of three configurations of h-BN. (a) bulk bilayer h-BN and in the presence of (b) open and (c) closed edges calculated from first principles. The structural transformations are schematically shown using the atomistic models.

relatively small curvature radii at the closed edges have very little effect on the band gap (4.3 eV). This finding is closely related to the calculations predicting nearly constant band gaps of BN nanotubes of different diameters [17–19].

In summary, utilizing a variety of atomically resolved imaging and spectroscopy techniques coupled with first-principles calculations, this study reveals new physical and chemical effects at the edges of h-BN. Subangstrom structural distortions and bonding changes result from the spontaneous formation of interlayer bonds at the edges of bilayer h-BN. Such structural distortions can significantly transform the electronic properties of h-BN flakes. Our spectroscopy results suggest an enhanced probability at the distortion for electrons to transition to π^* orbitals when excited, a behavior previously observed in carbon nanotubes and boron nitride sheets [16,20–22]. Although h-BN nanoribbons are predicted to show a metallic behavior locally at open edges, we demonstrate here that distortions arising from the covalent interlayer bonds across the bilayer h-BN can recover the insulating character of bulk bilayer h-BN. Such unusual bonding and local distortions across the edges in h-BN are strikingly different from graphene, and have been further rationalized using novel 3D orbital mapping. Functionalizing the edges in h-BN, through chemical vapor deposition of h-BN nanoribbons, for instance, can keep the edges open and result in a significantly different electronic behavior in this material. This study shows that small additional distortions in the atomic structure of the engineered nanocrystals can lead to peculiar physical, chemical, and electronic properties, which, if not understood properly, may hinder efforts to tailor materials' properties for desirable applications. Only by examining the engineered structure carefully, one atom at a time, and understanding the competing chemical and physical effects, can one successfully nanoengineer such materials.

*To whom correspondence should be addressed.
†qmramasse@superstem.org
‡azettl@berkeley.edu

[1] J.-H. Chen, L. Li, W. G. Cullen, E. D. Williams, and M. S. Fuhrer, Nat. Phys. **7,** 535 (2011).

[2] M. Schubert, B. Rheinländer, E. Franke, H. Neumann, T. E. Tiwald, J. A. Woollam, J. Hahn, and F. Richter, Phys. Rev. B **56,** 13 306 (1997).

[3] Y. W. Son, M. L. Cohen, and S. G. Louie, Nature (London) **444,** 347 (2006).

[4] H. Zeng, C. Zhi, Z. Zhang, X. Wei, X. Wang, W. Guo, Y. Bando, and D. Golberg, Nano Lett. **10,** 5049 (2010).

[5] Z. H. Zhang and W. L. Guo, Phys. Rev. B **77,** 075403 (2008).

[6] M. Topsakal, E. Akturk, and S. Ciraci, Phys. Rev. B 115442, **79** (2009).

[7] N. Alem, O. V. Yazyev, C. Kisielowski, P. Denes, U. Dahmen, P. Hartel, M. Haider, M. Bischoff, B. Jiang, S. G. Louie, and A. Zettl, Phys. Rev. Lett. **106,** 126102 (2011).

[8] O. L. Krivanek, M. F. Chisholm, V. Nicolosi, T. J. Pennycook, G. J. Corbin, N. Dellby, M. F. Murfitt, C. S. Own, Z. S. Szilagyi, M. P. Oxley, S. T. Pantelides, and S. J. Pennycook, Nature (London) **464,** 571 (2010).

[9] K. Suenaga and M. Koshino, Nature (London) **468,** 1088 (2010).

[10] L. P. Hansen, Q. M. Ramasse, C. Kisielowski, M. Brorson, E. Johnson, H. Topsøe, and S. Helveg, Angew. Chem., Int. Ed. **50,** 10 153 (2011).

[11] See Supplemental Material at http://link.aps.org/supplemental/10.1103/PhysRevLett.109.205502 for sample preparation, image and EELS recording condition, STEM image simulations, and first-principles calculations.

[12] O. L. Krivanek, N. Dellby, M. F. Murfitt, M. F. Chisholm, T. J. Pennycook, K. Suenaga, and V. Nicolosi, Ultramicroscopy **110,** 935 (2010).

[13] C. Collazo-Davila, E. Bengu, C. Leslie, and L. D. Marks, Appl. Phys. Lett. **72,** 314 (1998).

[14] L. Bourgeois, Y. Bando, K. Kurashima, and T. Sato, Philos. Mag. A **80,** 129 (2000).

[15] Y. Sun and J. Yuan, Phys. Rev. B **71,** 125109 (2005).

[16] E. Najafi, A. P. Hitchcock, D. Rossouw, and G. A. Botton, Ultramicroscopy **113,** 158 (2012).

[17] X. Blase, A. Rubio, S. G. Louie, and M. L. Cohen, Europhys. Lett. **28,** 335 (1994).

[18] R. Arenal, O. Stéphan, M. Kociak, D. Taverna, A. Loiseau, and C. Colliex, Phys. Rev. Lett. **95,** 127601 (2005).

[19] R. Arenal, X. Blase, and A. Loiseaua, *Advances in Physics: Boron-nitride and Boron-carbonitride Nanotubes: Synthesis, Characterization and Theory* (2010), Vol. 59, pp. 101.

[20] R. Arenal, M. Kociak, and N. J. Zaluzec, Appl. Phys. Lett. **90,** 204105 (2007).

[21] L. Bourgeois, Y. Bando, W. Q. Han, and T. Sato, Phys. Rev. B **61,** 7686 (2000).

[22] L. Bourgeois, Y. Bando, S. Shinozaki, K. Kurashima, and T. Sato, Acta Crystallogr. Sect. A **55,** 168 (1999).